Earth and Planetary Science Letters 541 (2020) 116295

Contents lists available at ScienceDirect

Earth and Planetary Science Letters

www.elsevier.com/locate/epsl

# Deciphering the evolution and forcing mechanisms of glaciation over the Himalayan-Tibetan orogen during the past 20,000 years

Qing Yan [a,b,*], Lewis A. Owen [c], Zhongshi Zhang [d,e], Nanxuan Jiang [a], Ran Zhang [f]

[a] Nansen-Zhu International Research Centre, Institute of Atmospheric Physics, Chinese Academy of Sciences, Beijing 100029, China
[b] Key Laboratory of Meteorological Disaster/Collaborative Innovation Center on Forecast and Evaluation of Meteorological Disasters, Nanjing University of Information Science and Technology, Nanjing 210044, China
[c] Department of Marine, Earth, and Atmospheric Science, North Carolina State University, Raleigh, NC 27695, USA
[d] Department of Atmospheric Science, School of Environmental Studies, China University of Geosciences, Wuhan 430074, China
[e] Uni Research Climate, Bjerknes Center for Climate Research, Bergen, Norway
[f] Climate Change Research Center, Institute of Atmospheric Physics, Chinese Academy of Sciences, Beijing 100029, China

ARTICLE INFO

*Article history:*
Received 2 September 2019
Received in revised form 7 March 2020
Accepted 19 April 2020
Available online 6 May 2020
Editor: L. Robinson

*Keywords:*
glaciation
Himalayan-Tibetan orogen
ice-sheet modeling
LGM

ABSTRACT

The evolution of past glaciations over the Himalayan-Tibetan orogen and their links with climate change remain elusive, partially owing to the immense scale of the orogen preventing the investigation of all areas. Numerical modeling aids in filling the gaps, verifying the geologic observations, and exploring forcing factors. Based on a transient climate-ice sheet simulation for the past 20 kyr, we demonstrate that the maximum extent of glaciation over the Himalayan-Tibetan orogen occurs around the last glacial maximum (LGM; defined here at ~20 ka), with expanded ice caps and extensive valley glaciers and being equivalent to a fourfold/sixfold expansion of today's glacier area/volume. The glacier extent shrinks rapidly after the LGM and reaches the minimum around ~8–7 ka, followed by a slight long-term advancing trend afterwards. Our results suggest a dominant role of summer temperature in controlling the overall trend of glacier response, with precipitation generally modulating the regional extent of glaciation. However, the timing and extent of glaciation in the simulations varies across the Himalayan-Tibetan orogen on millennial timescale, especially between the monsoon-influenced southern and westerly-influenced western parts, further confirming previous speculations based on glacial geologic records. Despite the uncertainties in the simulations and the discrepancy in glaciation between the simulations and the glacial geologic evidence (e.g., $^{10}$Be ages), our results provide additional clues on the relationship between climatic change and glacier response. In addition, the modeling aids in advancing our knowledge of the paleoglaciological history of the Himalayan-Tibetan orogen.



## 1. Introduction

The mountains of the Himalayan-Tibetan orogen hold the largest number of glaciers outside the polar regions, which feed numerous Asian rivers (e.g., Ganges, Indus, Yangtze, and Mekong) and provide crucial freshwater to billions of people (Pritchard, 2019). The cold environment benefiting from the high elevation helps sustain the glaciers, in tandem with precipitation brought by the south Asian monsoon and mid-latitude westerlies (Benn and Owen, 1998; Yao et al., 2012). The behavior of glaciers largely depends on the relative role of temperature and precipitation change. However, temperature and precipitation over the Himalayan-Tibetan orogen are known to respond to a variety of drivers and the relative importance of individual forcing factors varies spatially and temporally, leading to heterogeneous climate change and behavior of glaciers (e.g., Owen and Dortch, 2014; Yan et al., 2018; Saha et al., 2019). Deciphering the climatic controls on glacier fluctuations helps deepen our knowledge on present and future glacier evolution, which is, however, partially hampered by the short records of glacier observational data across the orogen. Extensive geologic evidence for past glaciations provides an avenue to help examine the links between climate change and glacier response in a long-term paleoclimate context and for aiding in understanding present and future changes.

Studies on the style and timing of late Quaternary glaciation over the Himalayan-Tibetan orogen have advanced considerably in the past few decades (Owen and Dortch, 2014, and refer-

* Corresponding author at: Nansen-Zhu International Research Centre, Institute of Atmospheric Physics, Chinese Academy of Sciences, 40 Huayanli, Chaoyang District, Beijing 100029, China.
*E-mail address:* yanqing@mail.iap.ac.cn (Q. Yan).

https://doi.org/10.1016/j.epsl.2020.116295
0012-821X/

ences therein). These studies are showing that during the last glacial (~110–16 ka), with glaciers in most regions reaching their maximum extent early in the last glacial, while in other areas glacial geologic evidence suggests the maximum glaciation occurring during the global last glacial maximum (gLGM; ~24–18 ka based on marine oxygen isotopes and sea levels [Mix et al., 2001]; see Sect. 2.5 for more discussions). However, vast areas of the Himalayan-Tibetan orogen were not glaciated during the last glacial, particularly during the gLGM when only expanded ice caps and extensive valley glaciers existed across the orogen (Shi, 2002; Owen and Dortch, 2014). A continental-scale ice sheet as proposed by Kuhle (1998) or seen in previous model simulations (Kirchner et al., 2011) did not exist. The restricted glaciation is attributed to the unfavorable climatic conditions during the gLGM (Yan et al., 2018), with insufficient cooling hampering large-scale glaciation over the eastern regions of the orogen, precipitation decrease preventing significant glacier advances over the northern regions of the orogen, and both insufficient cooling and precipitation decrease inhibiting glacier development over inner regions of the orogen. There were also multiple glacier advances since the gLGM across the Himalayan-Tibetan orogen (e.g. Dortch et al., 2013; Heyman, 2014; Murari et al., 2014; Saha et al., 2018, 2019), but the timing and extent of glaciation varies greatly between regions. The asynchronous glaciation likely results from the spatiotemporal variability of climate change and different climate sensitivity of glaciers (e.g., Owen and Dortch, 2014; Saha et al., 2019). Despite significant advances in numerical dating techniques, the chorological control is still relatively poor over the Himalayan-Tibetan orogen (e.g., individual age errors of 5–10%), especially before the gLGM, owing to the large geologic and physics uncertainties associated with the dating methods, and statistical analysis of ages (e.g., Owen and Dortch, 2014). Together with limited spatial coverage of glacial geologic evidence, these hamper the effort to construct convincing correlations in glaciation across the Himalayan-Tibetan orogen and to assess the relative importance of different climate systems, although regional correlations and tentative relationships are suggested by many studies (e.g., Dortch et al., 2013; Murari et al., 2014; Saha et al., 2018, 2019).

Through a transient climate-ice sheet simulation for the past 20 kyr when glacial geologic evidence becomes spatiotemporally more robust than older periods, we present a possible scenario for the evolution of glaciation over the Himalayan-Tibetan orogen, and identify the relative role of temperature and precipitation in forcing glacier advances. This is supported by (i) the quantitative/qualitative summer temperature and precipitation reconstructions (two of the dominant factors for glacier behavior) and (ii) the timing and extent of glaciation suggested by glacial geologic evidence (e.g., $^{10}$Be ages). Our study aims to advance our understanding of the interplay between climatic change and glacier response, which has important socioeconomic implications for evaluating the impacts of future climate change over high mountain Asia.

## 2. Methodology

### 2.1. Ice sheet model

We use the Parallel Ice Sheet Model (PISM), a three-dimensional, polythermal, thermodynamically coupled ice sheet model (Winkelmann et al., 2011), to examine glaciation across the Himalayan-Tibetan orogen. In the PISM, surface mass balance relies on the monthly surface air temperature and precipitation and is defined as the difference between accumulation and ablation. Accumulation is identical to precipitation when air temperature is below 0 °C and linearly reduces to zero when air temperature rises from 0 °C to 2 °C. Ablation is estimated by the positive-degree day scheme, with the melting rate of ice and snow being 8- and 3-mm-water equivalent $d^{-1}\,°C^{-1}$, respectively. A hybrid stress balance model is used to compute ice velocity, with the shallow ice and shelf approximations for vertical deformation and longitudinal stretching, respectively. The PISM also utilizes a pseudo-plastic power to calculate basal sliding.

The PISM has been proven effective for modeling ice sheets and ice fields in both past and present climates (e.g., Yan et al., 2016), although it may not be very suitable for smaller valley glaciers even at the 1-km-resolution considered here. However, the majority of the distributed glacier models have limited scope in modeling glaciers which grow into large ice caps and ice sheets and which existed before but are no longer present today (e.g., Maussion et al., 2019). We argue that the PISM is suitable for modeling glaciation since the gLGM, given the potential concurrence of ice sheets, ice caps and valley glaciers over the Himalayan-Tibetan orogen in the past.

### 2.2. Transient climate simulation

We use a transient simulation of the global climate for the past 22 kyr (referred to as TRACE) with the Community Climate System Model version 3 (CCSM3) (Liu et al., 2009). The CCSM3 consists four components coupled together: i) an atmospheric model (CAM3); ii) an oceanic model (POP); iii) a land model (CLM3); and iv) a sea ice model (CSIM3). The TRACE simulation is forced by realistic external forcing, which include orbital insolation, freshwater fluxes, ice sheets, and greenhouse gases (**Fig. S1**). The model reproduces the majority of the characteristics of the reconstructed climate during the past 22 kyr, such as high-latitude temperature and El Niño-Southern Oscillation (Liu et al., 2009, 2014). We use the monthly outputs of the TRACE simulation at a horizontal resolution of ~3.75° × 3.75°. Although the reconstructed ice sheets during the past 22 kyr serve as boundary conditions in the CCSM3, there is no ice prescribed over the Himalayan-Tibetan orogen in the model.

### 2.3. Transient glacier simulation

Here, we run the PISM at a 1 × 1 km resolution covering the Himalayan-Tibetan orogen with 3200 × 2000 grid points. The present-day topography is derived from global multi-resolution terrain elevation data of 2010 (Danielson and Gesch, 2011). The present-day air temperature is obtained from the High Asia Reanalysis at a resolution of 10–30 km (Maussion et al., 2014), with modern precipitation from the Tropical Rainfall Measuring Mission (TRMM) at a resolution of 0.25 × 0.25° (Huffman et al., 2007). These climatic forcing are then interpolated to the resolution of PISM using inverse distance weighting. The geothermal heat flux is set to 70 $mW/m^2$, within the range of observed heat flux across the Himalayan-Tibetan orogen and close to the average continental geothermal heat flux of ~60±12 $mW/m^2$ over China (Jiang et al., 2016). These settings are identical to those employed in Yan et al. (2018), which are proven to produce a close match in modern glacier distribution between observations and simulations with the PISM.

Next, we run the PISM continuously for 22,000 years at 1-km-resolution driven by the spatially-varied monthly climatic forcing from the TRACE to simulate the behavior of glaciers since the gLGM. We adopt the “anomaly” method to construct the climatic forcing used in the PISM owning to the coarse resolution of the CCSM3. Specifically, we add the standard anomalies for temperature and fractional anomalies for precipitation (computed from 1960–1990) from the TRACE to the baseline climatology in the PISM. We take the first 2,000 years as spin-up and analyze the results of the last 20,000 years. The climate simulation for the past 22 kyr is unique being a fully coupled transient simulation and

this ice sheet simulation performed here is also the first attempt of its kind. Note that extending the time frame back through the whole of the last glacial is hampered by the lack of spatially-varied climatic forcing and the huge cost of transient glacier simulation (e.g., a 1000-year-long run takes about five days using 480 cores on our cluster).

### 2.4. Geological evidence for climate and glaciation

We compile available geologic evidence for the Himalayan-Tibetan orogen (**Table S1 and Fig. S2**) that provides quantitative or qualitative information for temperature and precipitation during the past 20 kyr, as well as proxies for atmospheric circulations (e.g., Indian monsoon and mid-latitude westerlies). This helps to evaluate the performance of climate model in depicting the reconstructed climate change. Notably, the quantitative summer temperature reconstructions (e.g., Zhang et al., 2017), a dominant factor for glaciation, are extremely scarce over the orogen, so several proxies for temperature around the orogen are also used (e.g., Peterse et al., 2011). The history of the south Asian monsoon is reconstructed mainly based on speleothem $\delta^{18}$O from different caves (e.g., Fleitmann et al., 2007; Dutt et al., 2015; Kathayat et al., 2016) and $\delta^{18}$N from ocean sediments (Altabet et al., 2002), whereas it is measured in the model simulations as the zonal wind shear over the region of 10–25°N and 40–80°E during the peak precipitation season (Jun.–Sep.; Webster and Yang, 1992). The $\delta^{13}$C record from Sofular Cave (Fleitmann et al., 2009) is employed as a measure for the shift of the mid-latitude westerlies (Li et al., 2019), which, in the simulations, is defined as the zonal wind change between 25–40°N/50–80°E and 10–25°N/50–80°E.

The timing and extent of glaciation over the Himalayan-Tibetan orogen during the past 20 kyr is mainly based on previous compilations of $^{10}$Be ages that approximate the time of deglaciation and the reconstructed equilibrium-line altitudes (ELAs). Specifically, for the gLGM, we select the sites where glacier advances have recognized and dated using $^{10}$Be cosmogenic nuclides to ~28–15 ka (Owen and Dortch, 2014; also see Table S6 in Yan et al. (2018) for details). The reconstructed ELA depressions (~337±197 m; Heyman, 2014) and/or the total length of former glaciers (Owen and Dortch, 2014; Yan et al., 2018) suggest expanded ice caps and extensive valley glaciers across the orogen during the gLGM. Regarding the evolution of glaciation since the gLGM, Dortch et al. (2013) compiled 692 $^{10}$Be ages across the semi-arid western Himalayan-Tibetan orogen and defined eight regional glacial stages (~20±2, 16.9±0.7, 14.9±0.8, 13.9±0.5, 12.2±0.8, 3.8±0.6, 1.7±0.2, and 0.4±0.1 ka) for which a significant and datable glacial advance occurs in more than one mountain range. Similarly, Saha et al. (2018) defined seven Holocene regional glacial stages for the northwestern end of the orogen, which date to ~10.9–9.3, 8.2–7.4, 6.9–4.3, 4.5–2.8, 2.7–1.8, 1.8–0.9, and <1 ka. Over the monsoon-influenced regions of the orogen, Murari et al. (2014) established twenty-seven regional glacial stages, including 11 stages during the Holocene (from ~11.4±0.7 to 0.4±0.1 ka). Furthermore, Saha et al. (2019) defined local glacial stages for five climatic zones across the Himalayan-Tibetan orogen and suggested at least one Lateglacial (~15.3–11.8 ka) and five Holocene regional glacial stages (~11.5–9.5, 8.8–7.7, 7.0–3.2, 2.3–1.0, and <1 ka). Saha et al. (2019) reconstructed the extent of glacier advances in 77 glaciated valleys using ELAs **(Table S2)**. Additionally, Blomdin et al. (2016) suggested only one reliable regional glacial stage at ~28–15 ka across the Tian Shan based on statistical analyses on sets of $^{10}$Be ages. In the model simulations, we define regional glacial stage as the interval when regionally-averaged glacierized area is larger than present and the extent is measured by the total glacier area.

### 2.5. The timing of the gLGM

The timing and duration of the gLGM varies between studies depending on the different proxies. The gLGM is defined by Mix et al. (2001) as a chronozone spanning from ~24 to 18 ka on the basis of global marine oxygen isotopes and sea levels, whereas Hughes and Gibbard (2015) defined the gLGM as the interval covering ~28–23 ka based on global dust concentration for a clear stratigraphical basis. Furthermore, Clark et al. (2009) used global radiocarbon/cosmogenic surface exposure ages to define the gLGM as between ~27 and 19 ka. Given the limited length of the TRACE simulation and the 2-kyr spin-up, we define the gLGM here at ~20 ka, corresponding to the timing of maximum glacier extent in our simulations, which broadly fits the definitions of Clark et al. (2009) and Mix et al. (2001), and is consistent with the regional glacial stages identified over the Himalayan-Tibetan orogen (i.e., 20±2 ka or 22±2 ka; Dortch et al., 2013; Murari et al., 2014). Additionally, we broadly define the Oldest Dryas as the interval spanning ~18–15 ka, the Bølling–Allerød at ~15–13 ka, and Younger Dryas at ~13–11.5 ka, given the fact that the definitions of chronozones may depend on the geological evidence used (e.g., $\delta^{18}$O from Greenland ice cores [Johnsen et al., 1997]).

## 3. Glaciation across the Himalayan-Tibetan orogen

In the PISM transient simulation, the maximum extent of glaciation occurs at ~20–18 ka, close to the timing of the gLGM (~24–18 ka or ~27–19 ka; Mix et al., 2001; Clark et al., 2009), with the total glacier area approximately quadrupled (**Fig. 1c**). The most extensive glaciation at ~20 ka is located at the western parts of the Himalayan-Tibetan orogen, including western Tibet, Pamir, and Tian Shan (**Fig. 1g**). Glacier advances are relatively restricted over the southern Tibet, Hengduan Mountain, and Qilian Mountain. In contrast, the majority of central and eastern Tibet remains ice free at ~20 ka. The modeled glacier distribution is broadly consistent with the glacial geologic evidence suggesting expanded ice caps and extensive valley glaciers (Owen and Dortch, 2014; Heyman, 2014) and a fourfold expansion of modern glacier area (Shi, 2002) during the gLGM, as well as the simulated glaciation based on the PMIP3 models (Yan et al., 2018). However, the extent of glaciation over some regions is overestimated, e.g., several glaciers over Pamir and Tian Shan have advanced <10 km (Xu et al., 2010; Lifton et al., 2014), where ice fields/caps develop in the simulations. Additionally, the maximum glacier volume, ~5 times greater than present, is reached around 18 ka (**Fig. 1e**). This indicates asynchronous timing of maximum glacier extent and volume over the Himalayan-Tibetan orogen during the past 20 kyr, which is also found in the evolution of the Northern Hemisphere ice sheets (e.g., Lecavalier et al., 2014).

The extent of glaciation shrinks rapidly over the Himalayan-Tibetan orogen after the gLGM (~20–18 ka in the model), which is consistent with the timing of deglaciation suggested by $^{10}$Be ages (~18–16 ka; Clark et al., 2009) and closely follows the variation of regional summer temperature (**Figs. 1a, c**). The retreating rate is relatively faster from ~18 to 14 ka than for the period at ~14–11 ka (**Fig. 1d**). This is attributed to the slower summer warming and enhanced precipitation during the later interval (**Figs. 1a, b**). The total glacier area begins to fall below the present-day level in the first part of the Early Holocene (at ~11 ka), when the summer temperature is significantly warmer than today that is supported by multi-proxies (Peterse et al., 2011; Zhang et al., 2017). This is followed by a long-term upward trend during the Holocene, largely arising from a decrease in summer temperature. The total glacier area recovers to modern level at ~2 ka and keeps increasing until industrial times (~0.3 ka), after which the modern warming leads to an accelerated melting of glaciers (**Figs. 1c, d**). This evolution-

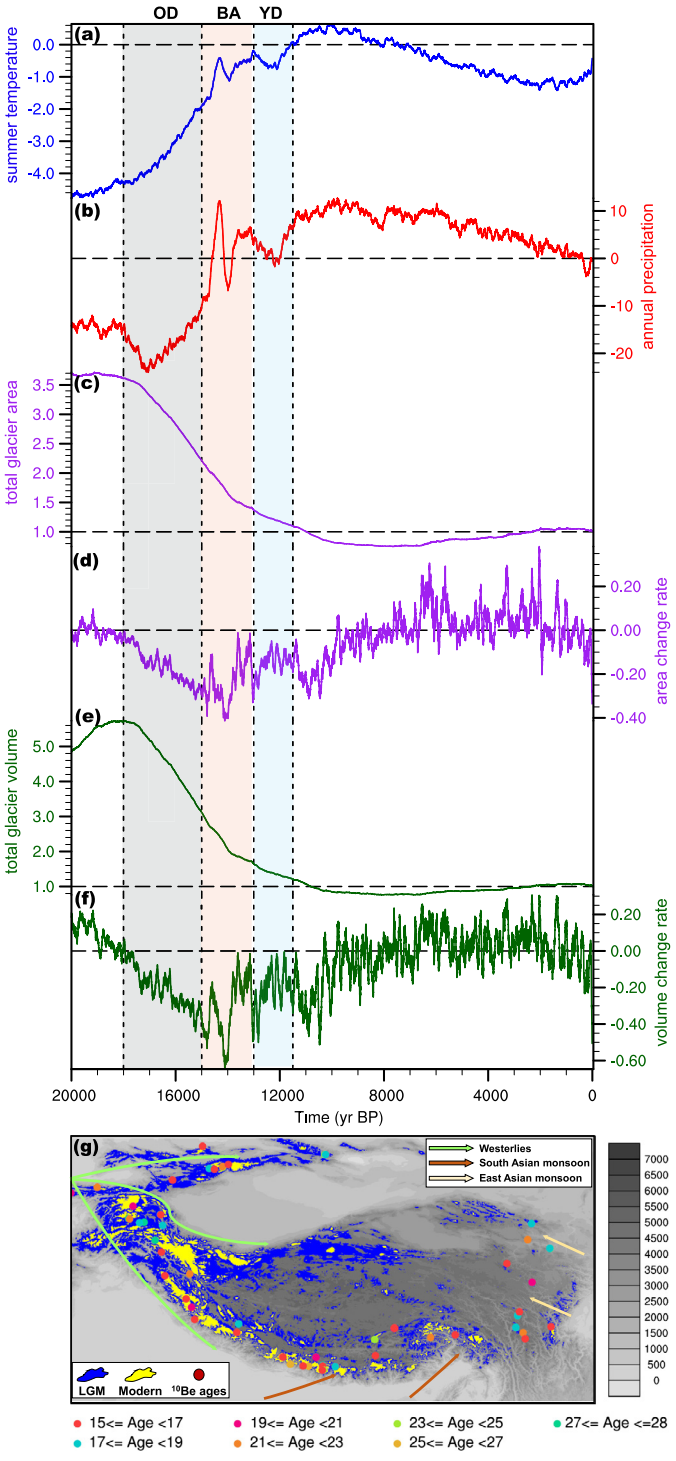


**Fig. 1. Modeled evolution of climate and glaciation over the Himalayan-Tibetan orogen for the past 20 kyr.** (a) Anomaly of summer temperature relative to present (°C). (b) Fractional change of annual mean precipitation relative to present (%). (c, e) Ratio of (c) total glacier area and (e) volume to present level. Ratio >1 and <1 indicates glacier larger and smaller than present, respectively. (d, f) Change rate (‰/yr) of (d) total glacier area and (f) volume. Positive (negative) values indicate glacier advance (retreat) relative to previous year. The vertical shadings show the Oldest Dryas (OD), Bølling-Allerød (BA), and Younger Dryas (YD). (g) The modeled glacier distribution during the LGM (at ~20 ka) and present. The dots show the sites where glacier advances have recognized for the LGM and dated using $^{10}$Be cosmogenic nuclides to ~28–15 ka (see Table S6 in Yan et al. (2018) for details). Arrows are the schematic locations and directions of different climate systems. (For interpretation of the colors in the figure(s), the reader is referred to the web version of this article.)

ary pattern of glaciation, with a maximum around the gLGM and a long-term decreasing trend afterwards, is also observed in the variation of total glacier volume (**Figs. 1e, f**) and shares large similarity with the change in the Greenland ice sheet (Lecavalier et al., 2014; Buizert et al., 2018). However, the glacier evolution may vary over different climatic-topographic regions of the Himalayan-Tibetan orogen as suggested by glacial geologic evidence (Owen and Dortch, 2014), which is hence further examined and compared with glacial records below.

### 3.1. Southern parts of the Himalayan-Tibetan orogen

Over the southern parts of the Himalayan-Tibetan orogen (**Fig. 2h**), the modeled summer temperature exhibits an upward trend during the Oldest Dryas (~18–15 ka), with an increase in precipitation arising from the strengthening south Asian monsoon (**Figs. 2a–c**). This is confirmed by the reconstructed temperatures from loess–paleosol sequences (Peterse et al., 2011) and subfossil chironomids (Zhang et al., 2017), precipitation from pollens (Chen et al., 2014) and speleothem $\delta^{18}$O (Kathayat et al., 2016), and monsoon intensity from marine $\delta^{15}$N (Altabet et al., 2002) and speleothem $\delta^{18}$O (Fleitmann et al., 2007; Dutt et al., 2015). The summer warming leads to the profound deglaciation over the Oldest Dryas (**Figs. 2f, g**), which is supported by the anomalously low $\delta^{18}$O values in the northernmost Bay of Bengal that are indicative of enhanced meltwater runoff (Weldeab et al., 2019). Despite rapidly melting, the glacier extent during the Oldest Dryas is still larger than today (**Fig. 2f**), consistent with the compiled $^{10}$Be ages suggesting glacier advances at 18.7±1.8 to 15.5±1.3 ka (**Fig. 2d**; Murari et al., 2014). There is then an obvious glacier development (~1.5 times expansion) during the Bølling-Allerod (~15–13 ka), confirmed by the reconstructed ELA depressions (~1061±273 m) at that time (**Fig. 2e**). This advance is largely attributed to the enhanced south Asian monsoon and hence more precipitation (**Figs. 2a–c**), which overwhelms the increased summer melting resulting from rising temperature. Summer temperature exhibits a slight decrease during the Younger Dryas (~13–11.5 ka), whereas precipitation is greatly reduced due to the weakened South Asian monsoon as indicated by both simulations and reconstructions (**Figs. 2a–c**). The reduction in precipitation contributes largely to the retreat of glaciers during the Younger Dryas (**Figs. 2f, g**), matching with the reconstructed larger meltwater runoff in the northernmost Bay of Bengal (Weldeab et al., 2019). However, the extent of glaciation remains larger than today (with a ratio of ~1.4; **Fig. 2f**), consistent with the complied $^{10}$Be ages suggesting glacier advances in some areas during the Younger Dryas and the reconstructed ELA depressions of 625 ± 455 m at 13.0–10.9 ka (**Figs. 2d, e;** Murari et al., 2014; Saha et al., 2019).

There is a decreasing trend in glacier area during the Early Holocene (11.7–8.2 ka) over the southern parts of the orogen, arising from the higher summer temperature that exceeds the role of enhanced precipitation from stronger south Asian monsoon (**Figs. 2a–c**). Notably, the extent of glacier during the Early Holocene (especially the early part) remains larger than today, which results mainly from cooler summer temperature (**Fig. S3**) due to increased cloudiness and evaporation, though with higher insolation (Rupper et al., 2009). The larger glacier area is broadly consistent with the geological evidence indicating glacier advances during the Early Holocene (**Figs. 2d, e**), e.g., the modeled glacierized area is ~10% larger than present and the reconstructed ELAs depressions are 330 ± 180 m at 9.5–8.7 ka (Saha et al., 2019). The glacier extent keeps above the present-day level during the Mid- and Late Holocene (8.2–0 ka) owing to the modeled lower summer temperature (**Fig. 2a**), with enhanced glacier expansion during several time intervals indicated by larger positive changing rate (**Figs. 2f, g**), which is broadly in agreement with the glacial records

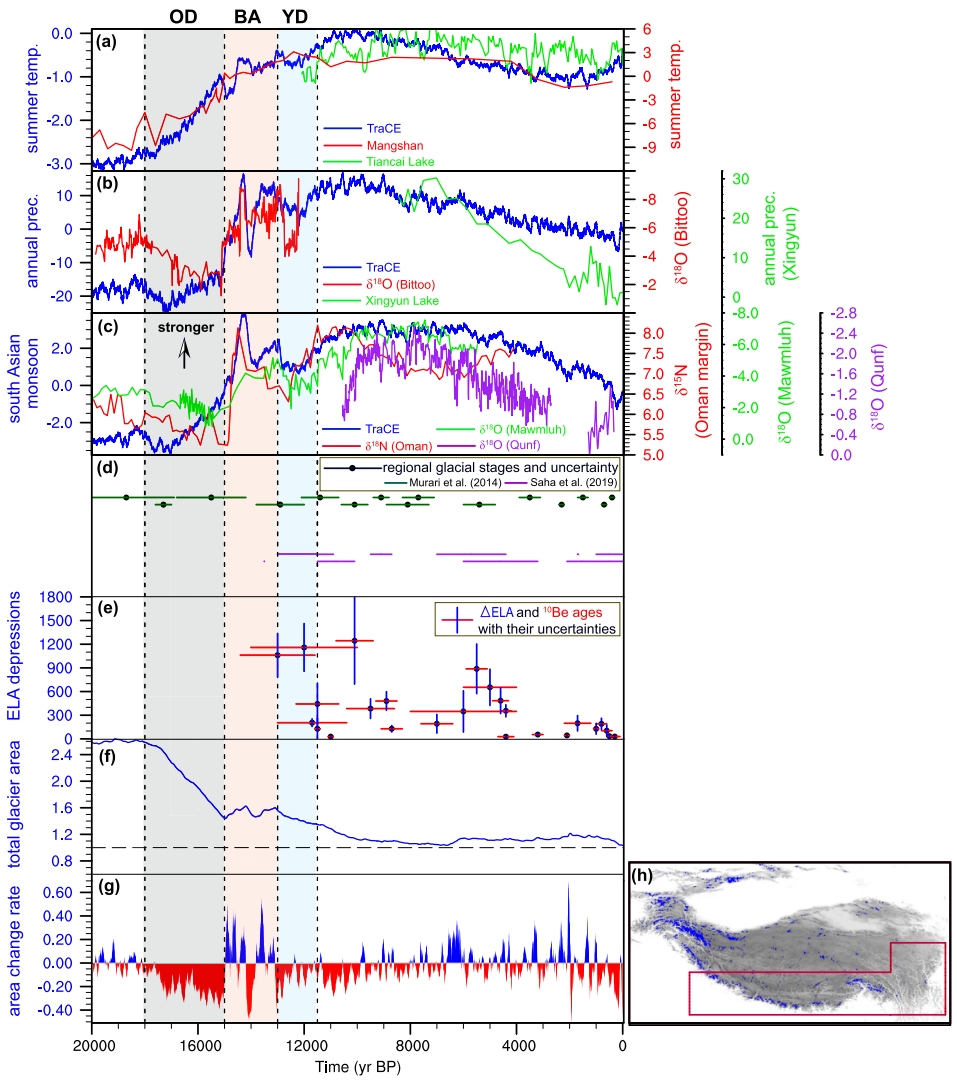


**Fig. 2. The evolution of climate and glaciation over the southern parts of the Himalayan-Tibetan orogen for the past 20 kyr.** (a) Summer temperature anomaly (°C) based on the TRACE and the reconstructions at Tiancai Lake (Zhang et al., 2017) and Mangshan loess plateau (Peterse et al., 2011). (b) Annual mean precipitation change (%) based on the TRACE and the reconstruction at Xingyun Lake (Chen et al., 2014), as well as the $\delta^{18}$O record from Bittoo cave (Kathayat et al., 2016). (c) Intensity of the south Asian monsoon based on the TRACE (m/s), the $\delta^{15}$N records at the Oman Margin (Altabet et al., 2002), and the $\delta^{18}$O records at the Mawmluh Cave (Dutt et al., 2015) and Qunf Cave (Fleitmann et al., 2007). Note that more information about the climatic proxies used here is given in Table S1. (d) Regional glacial stages and their uncertainties based on the compiled $^{10}$Be ages (Murari et al., 2014; Saha et al., 2019). Note that the reconstructed glacial stages are shown in multiple rows for better readability and regional glacial stages in Saha et al. (2019) are from climatic zones 2b&3 defined in their study. (e) Timing and amplitude of regional glacier advances based on the reconstructed ELA depressions and $^{10}$Be ages (climatic zones 2b&3 in Saha et al. (2019); Table S2). (f) Ratio of the modeled total glacier area to present level. (g) Change rate (‰/yr) of the modeled glacier area. (h) The southern parts of the Himalayan-Tibetan orogen defined here (red rectangular). The vertical shadings show the Oldest Dryas (OD), Bølling-Allerød (BA), and Younger Dryas (YD).

indicating multiple glacier advances (**Figs. 2d, e**). For example, the reconstructed ELAs reduce by ~300–900 m at ~7–5 ka (**Fig. 2e**), when an obvious glacier development (i.e., positive changing rate) is also seen in the model (**Figs. 2f, g**). These intense glacier advances generally benefit from enhanced precipitation, in tandem with lower summer temperature based on our simulation (**Fig. S4**).

### 3.2. Western parts of the Himalayan-Tibetan orogen

Over the western parts of the Himalayan-Tibetan orogen (**Fig. 3h**), the negative changing rate indicates a continuous retreat of glaciers from the Oldest Dryas to Younger Dryas (**Figs. 3f, g**). This deglaciation is largely forced by the modeled rising summer temperature that broadly matches with the alkenone/pollen-based temperatures (Jiang et al., 2013; Zhao et al., 2017), with precipitation, regulated by the meridional shift of the mid-latitude westerlies, only affecting the amplitude of the melting rate (**Figs. 3a–c**). Precipitation is greatly enhanced during the Bølling-Allerod, e.g., resulting from the poleward shift of the mid-latitude westerlies, confirmed by geologic evidence (i.e., $\delta^{13}$C and leaf wax $\delta$D; Fleitmann et al., 2009; Hou et al., 2017), which is but not enough to offset the increased summer ablation due to higher temperature. Despite significant melting, glaciation remains more extensive than present from the Oldest Dryas to Younger Dryas (~18–11.5 ka), after which the modeled glacierized area tends to fall below present level (**Fig. 3f).** This is consistent with the compilations of $^{10}$Be ages and the reconstructed ELAs suggesting multiple glacier advances during this period (**Figs. 3d, e**). For example, glacial records suggest extensive advances during the Bølling-Allerod and Younger Dryas with progressively restricted extent (in terms of ELA depressions; **Fig. 3e**), which is well depicted in the model showing restricted glaciation through time (i.e., the ratio of total glacier area to present level decreases from ~2.2 to 1.0; **Fig. 3f**).

Notably, the higher summer temperature in the early part of the Early Holocene (~11–10 ka) leads to enhanced melting and a

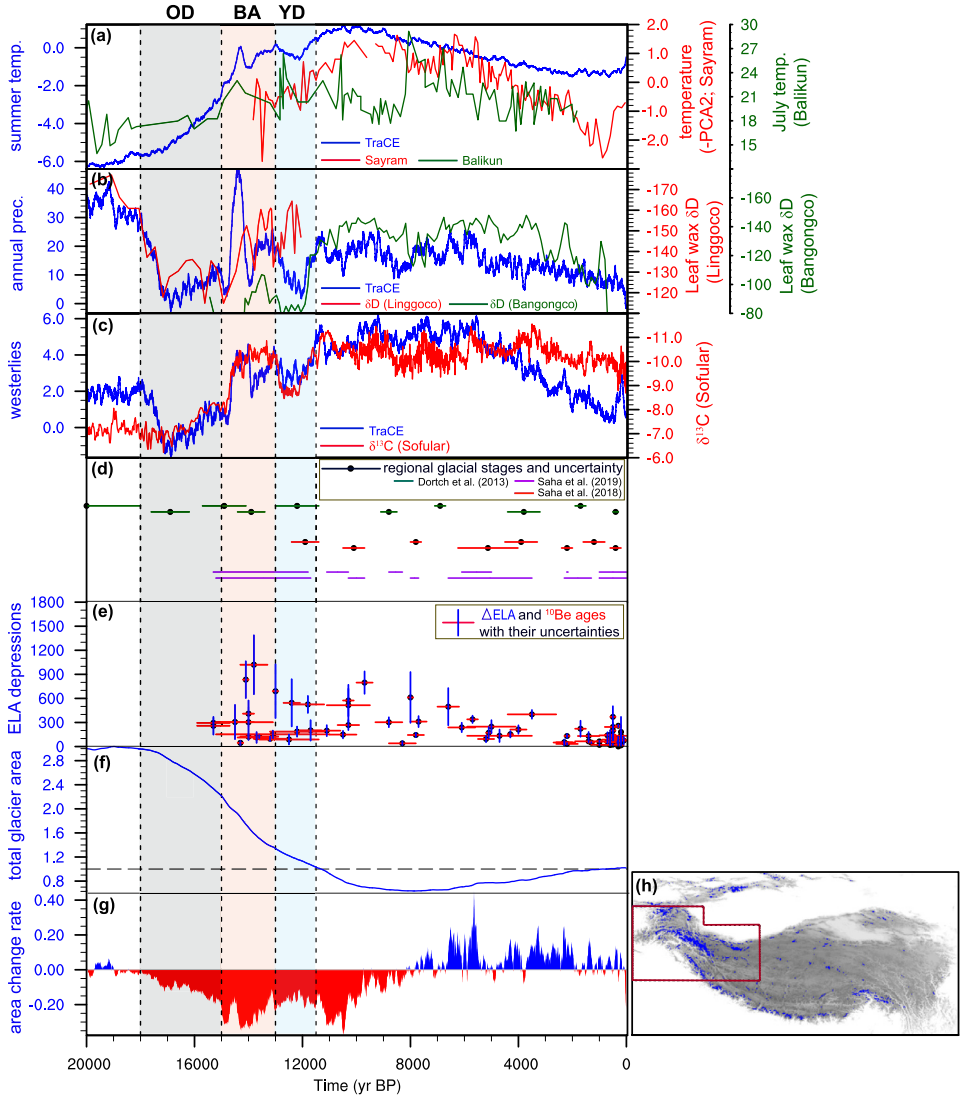


**Fig. 3. The evolution of climate and glaciation over the western parts of the Himalayan-Tibetan orogen for the past 20 kyr.** (a) Summer temperature anomaly (°C) based on the TRACE and the reconstruction at Balikun Lake (Zhao et al., 2017), as well as qualitative temperature reconstruction from the Sayram Lake (Jiang et al., 2013). (b) Annual mean precipitation change (%) based on the TRACE and the leaf wax $\delta$D (an indicator for precipitation) from Linggoco and Bangongco (offset by +70; Hou et al., 2017). (c) Meridional shift of the mid-latitude westerlies based on the TRACE (m/s) and the $\delta^{13}$C record from Sofular Cave (Fleitmann et al., 2009). Note that more information about the climatic proxies used here is given in Table S1. (d) Regional glacial stages and their uncertainties based on the compiled $^{10}$Be ages (Dortch et al., 2013; Saha et al., 2018, 2019). Note that the reconstructed glacial stages are shown in multiple rows for better readability and regional glacial stages in Saha et al. (2019) are from climatic zones 1a&2a defined in their study. (e) Timing and amplitude of regional glacier advances based on the reconstructed ELA depressions and $^{10}$Be ages (climatic zones 1a&2a in Saha et al. (2019); Table S2). (f) Ratio of the modeled total glacier area to present level. (g) Change rate (‰/yr) of the modeled glacier area. (h) The western parts of the Himalayan-Tibetan orogen defined here (red rectangular). The vertical shadings show the Oldest Dryas (OD), Bølling-Allerød (BA), and Younger Dryas (YD).

shrinkage of glacier extent below present-day level. This is confirmed by the modeling results of Rupper et al. (2009) suggesting higher equilibrium-line altitudes over the western Central Asia and the higher lake-level in western Tibet likely due to melting glaciers (Kong et al., 2007). However, it is in sharp contrast to the reconstructions that show extensive advances during the latest part of the Early Holocene and possibly into the early part of the Mid-Holocene (**Figs. 3d, e and Fig. S5**). Although the modeling shows clear development of glaciers (i.e., positive changing rate) after the end of the Early Holocene (~8 ka) because of the decreasing summer temperature (**Figs. 3a, f, g**), the extent of glaciation remains below present-day level, inconsistent with the glacial geologic records suggesting a lowering of ELAs (**Fig. 3e**). While the reconstructed glacial advances during the last millennium are captured in the model showing larger glacier extent than present-day, though with potential discrepancy in the timing.

### 3.3. Northern parts of the Himalayan-Tibetan orogen

Over the Tian Shan, the model predicts significant glacier advances relative to present from the gLGM to Bølling-Allerod (~20–13 ka), but with progressively restricted glaciation (**Figs. 4b, c**). The extent of glaciation falls below present level after ~13 ka and reaches the minimum around ~8 ka, which is followed by a slight long-term advancing trend afterwards. The simulated timing of glaciation matches with the glacial geologic evidence ($^{10}$Be ages) suggesting regional glacier expansions mainly occurring between 28 and 15 ka (Blomdin et al., 2016; **Fig. 4a**). The limited large-scale glaciation during the Early-Mid Holocene is largely attributed to the higher summer temperature in our simulations (**Fig. S6**), though glacier advances are observed in individual valleys during the Neoglacial (Xu et al., 2010). The evolution of glaciation over the Central Kunlun shares large similarity with the glacier behavior over the Tian Shan, with a maximum at ~20 ka and a minimum at

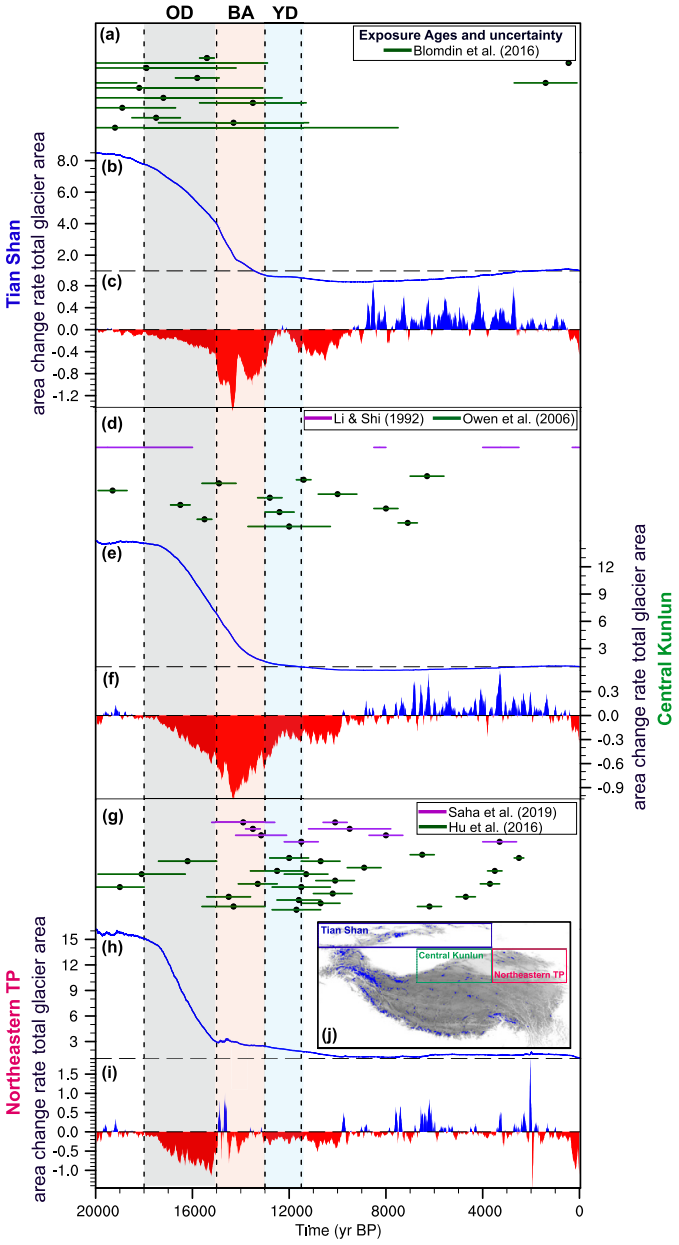


**Fig. 4. The evolution of climate and glaciation over the northern parts of the Himalayan-Tibetan orogen for the past 20 kyr.** (a-c) Timing of glacier advances based on the compiled $^{10}$Be ages (a; Blomdin et al., 2016), the ratio of the modeled total glacier area to present level (b), and change rate (‰/yr) of the modeled glacier area (c) across Tian Shan. Note that the $^{10}$Be ages are shown in multiple rows for better readability. (d-f) same as (a-c) but for Central Kunlun. The timing of glacier advances in (d) is based on the individual $^{10}$Be ages from Owen et al. (2006) and the $^{14}$C dating from Li and Shi (1992). (g-i) same as (a-c) but for Northeastern Tibetan Plateau. The timing of glacier advances in (g) is based on the individual $^{10}$Be/OSL ages from Hu et al. (2016, and references therein) and from Saha et al. (2019; climatic zone 1b). (j) The northern parts of the Himalayan-Tibetan orogen defined here (blue for Tian Shan, green for central Kunlun, and pink for northeastern Tibetan Plateau). The vertical shadings show the Oldest Dryas (OD), Bølling-Allerød (BA), and Younger Dryas (YD).

~8 ka (**Figs. 4e, f**). This is generally consistent with the $^{10}$Be ages that indicate multiple glacier advances from the gLGM to Younger Dryas (**Fig. 4d**), but the model fails to reproduce glaciation during the Early to Mid-Holocene evident in several individual valleys (e.g., Owen et al., 2006).

For the northeastern Tibet where precipitation is broadly dominated by the East Asian monsoon, the glaciers behave similarly to those over the southern parts of the Himalayan-Tibetan orogen (**Figs. 4h, i**), with a maximum at ~20 ka and a long-term decreasing trend afterwards. The modeled progressively restricted glaciation during the past 20 ka is supported by the reconstructed ELAs showing smaller ELA depressions with time (e.g., Saha et al., 2019). Moreover, the significant development of glaciers during the Bølling-Allerod and Younger Dryas (i.e., ~15–11.5 ka) indicated by the complied $^{10}$Be ages is well captured in the simulations (**Figs. 4g, h**), which results from the enhanced precipitation due to the stronger Asian summer monsoon and summer cooling, respectively (**Fig. S6**). In contrast to the Tian Shan and Central Kunlun, glacier development is observed during the Early to Mid-Holocene over the northeastern Tibet, with the glacierized area 20–30% larger than present (**Fig. 4h**). This is tied to the increased precipitation over the northeastern Tibet from stronger summer monsoon during the Early to Mid-Holocene that overwhelms the role of summer warming (**Fig. S6**).

Clear regional difference in the extent of glaciation emerges in the comparison of the simulated glacier behavior between the monsoon-influenced and westerly-influenced parts of the Himalayan-Tibetan orogen (e.g., southern vs. western parts). In the PISM simulation, the western parts of the orogen experience extensive glacier advances during the cold gLGM, while glaciation is relatively restricted over the southern parts of the orogen (**Fig. 1g**). This regional discrepancy is partially attributed to the fact that precipitation is greatly reduced over the southern parts of the orogen arising from the weakened south Asian monsoon (**Figs. 2b, c**), limiting large-scale glaciation. Whereas the northward shift of mid-latitude westerlies favors higher precipitation over the western parts of the orogen (**Figs. 3b, c**) and hence more intense glaciation. Alternatively, the larger temperature depressions over the western parts of the orogen than the southern parts may also contribute to the more extensive glaciation over the western parts during the gLGM (~20 ka). Additionally, there are obvious glacier advances over the southern parts of the orogen during the Bølling-Allerod, whereas the western parts of the orogen experiences little glacier development (**Figs. 2g, 3g**). Given enhanced precipitation and higher temperature over the two regions (**Figs. 2, 3**), this difference in glaciation may partially result from different sensitivity of glaciers: glaciers over the southern (monsoon-influenced) and western (westerly-influenced) parts of the orogen are more sensitive to precipitation and temperature, respectively, as suggested by Murari et al. (2014). During the Early Holocene, glacier advances are restricted in the southern parts of the orogen relative to present, whereas glacier retreats are evident in the western parts (**Figs. 2f, 3f**). This is attributed to the difference in summer temperature, which is broadly warmer and cooler than the present in the western and southern parts of the orogen (**Fig. S3**), respectively. Overall, the extent and timing of glaciation vary greatly across the orogen, likely caused by the spatiotemporal variability of temperature/precipitation change and different sensitivity of glaciers.

## 4. Discussions

The PISM reproduces several key features of glaciation for the past 20 kyr over the Himalayan-Tibetan orogen in comparison with glacial geologic evidence, but the model-data discrepancy still exists. The overall extent of glaciation over the western parts of the orogen is overestimated during the LGM, though extensive glacier advances were recorded in several individual glaciers. Another mismatch case is that the reconstructed extensive glaciation in the latter part of the Early Holocene (Dortch et al., 2013; Murari et al., 2014; Saha et al., 2018, 2019) is not well captured in our simulation, especially over the western parts of the orogen where the model predicts glacier retreat, as the rising summer temperature as revealed by proxies is unfavorable for large-scale glaciation. Besides, the model does not predict extensive glacier advances during

the abrupt cold events (e.g., Younger Dryas), which may be partially attributed to the fact that the abrupt cooling is mostly a winter phenomenon (e.g., Buizert et al., 2018; **Fig. S7**) and the corresponding decrease in precipitation dominates the mass balance of glaciers. Even for the glacier advances seen in both simulations and reconstructions, the extent and timing of glaciation still differ.

The model-data discrepancies may be attributed to the uncertainties in the climatic forcing, ice sheet model, and geologic evidence. First, the CCSM3 model is broadly capable to depict the reconstructed large-scale climatic signal (e.g., the south Asian summer monsoon) for the past 20 kyr, but it shows limited skill in reproducing the magnitude of climate change over the Himalayan-Tibetan orogen and the very short-term climate events. Meanwhile, the horizontal resolution of the CCSM3 is too coarse to capture the microclimatic variations within individual mountain ranges, which are potentially important for glaciation (Owen and Dortch, 2014). Thus, using a high-resolution regional climate model that enables more explicitly resolved physical and dynamical processes could provide more detailed climatic information across the Himalayan-Tibetan orogen, but this requires enormous computer resources. Second, the 1-km-resolution PISM may be still inefficient to resolve the ice geometry of individual glaciers. Uncertainties in model parameterizations (e.g., positive-degree day and the associated values) and missing processes could affect the simulated glacier extent. These uncertainties are not quantified owing to the huge computational expense of transient simulation, but the pattern of glacier response may largely be unchanged (e.g., Rupper et al., 2009; Yan et al., 2018). Besides, as the modeled glacier responds very quickly to the imposed climatic forcing (**Fig. S8**), we argue that the 2-kyr spin-up applied here may have limited influence on the modeled regional glaciation during the past 20 kyr. Overall, the CCSM3 and PISM used here produce valuable information on the evolution of regional glaciation, but are not capable of uncovering the behavior of individual glaciers.

Lastly, there are uncertainties in defining the timing of glaciation based on glacial landforms and sediments, owing to various correction schemes in numerical dating, geologic error, as well as statistical treatment of ages (Owen and Dortch, 2014; Saha et al., 2018, 2019). For example, the recorded Early Holocene glaciation might be more coincident with the 8.2 ka cooling event, rather than significant advances throughout the Early Holocene. Meanwhile, the exposure age approximates the time of deglaciation and provides no information on the duration of glacier advances. The immense scale of the orogen and problems associated with preservation of moraines hamper the efforts to construct a spatiotemporal distribution of glaciation over the Himalayan-Tibetan orogen and hence detailed model-data comparison. Additionally, the scarcity of quantitative proxies for summer temperature and precipitation across the orogen largely hampers a comprehensive evaluation of the model results, hence limiting our efforts to identify the key climatic factors responsible for the glaciation suggested by glacial records. Nevertheless, this modeling and the comparisons with the geologic data show the strong controls of the climatic systems on the spatial extent and timing of glaciation. This highlights the challenges of predicting future changes in glaciation, suffice to say we should expect wide and varying glacier responses to future climate change.

## 5. Summary

Based on a transient climate-ice simulation, we find that the maximum extent of glaciation for the past 20 kyr occurs around the LGM (as defined at ~20 ka), being equivalent to a fourfold (sixfold) expansion of today's glacier area (volume). As the glacial geologic evidence (mainly $^{10}$Be ages and ELAs) suggests, the model predicts expanded ice caps and extensive valley glaciers over the Himalayan-Tibetan orogen in the LGM, with ice-free condition in the interior, though the extent of glaciation may be overestimated by the modeling in some regions. The extent of glaciation shrinks rapidly after the LGM and reaches the minimum around ~8–7 ka, followed by a slight long-term advancing trend afterwards. Our results indicate a dominant role of summer temperature in controlling the overall evolution of glaciation during the past 20 ka, with precipitation modulating the extent and change rate. Additionally, the timing and extent of glaciation varies across the Himalayan-Tibetan orogen on millennial timescales, especially between the western and southern parts of the orogen, which may be attributed to the different dominant climate systems, spatiotemporal variability of climate change, and climate sensitivity of glaciers.

Although there are caveats to be considered, we, for the first time, present a possible modeled scenario on the evolution of glaciation over the Himalayan-Tibetan orogen for the past 20 kyr, and provides additional clues on the relationship between climate forcing and glacier response. Our results may advance our knowledge on the paleoglaciological history of the Himalayan-Tibetan orogen and have important socioeconomic implications for assessing the impacts of future climate change in the region.

## Declaration of competing interest

The authors declare that they have no known competing financial interests or personal relationships that could have appeared to influence the work reported in this paper.

## Acknowledgements

We thank Robin Blomdin and an anonymous reviewer for the constructive comments, which help greatly improve the quality of the paper. This study was supported by the Second Tibetan Plateau Scientific Expedition and Research program (2019QZKK0101), the Youth Innovation Promotion Association by CAS (2019080), and the Young Elite Scientists Sponsorship Program by China Association for Science and Technology (2017QNRC001). The PISM model can be downloaded at http://www.pism-docs.org and is supported by NASA grants NNX13AM16G and NNX13AK27G. The TRACE simulation is available at https://www.earthsystemgrid.org/project/trace.html. The modeled total glacier area from PISM is available at the supplementary material.

## Appendix A. Supplementary material

Supplementary material related to this article can be found online at https://doi.org/10.1016/j.epsl.2020.116295.

## References

Altabet, M.A., Higginson, M.J., Murray, D.W., 2002. The effect of millennial-scale changes in Arabian Sea denitrification on atmospheric CO2. Nature 415 (6868), 159–162.

Benn, D.I., Owen, L.A., 1998. The role of the Indian summer monsoon and the mid-latitude westerlies in Himalayan glaciation: review and speculative discussion. J. Geol. Soc. 155 (2), 353–363. https://doi.org/10.1144/gsjgs.155.2.0353.

Blomdin, R., Stroeven, A.P., Harbor, J.M., Lifton, N.A., Heyman, J., Gribenski, N., et al., 2016. Evaluating the timing of former glacier expansions in the Tian Shan: a key step towards robust spatial correlations. Quat. Sci. Rev. 153, 78–96.

Buizert, C., Keisling, B.A., Box, J.E., He, F., Carlson, A.E., Sinclair, G., DeConto, R.M., 2018. Greenland-wide seasonal temperatures during the last deglaciation. Geophys. Res. Lett. 45 (4), 1905–1914.

Chen, F., Chen, X., Chen, J., Zhou, A., Wu, D.U.O., Tang, L., et al., 2014. Holocene vegetation history, precipitation changes and Indian Summer Monsoon evolution documented from sediments of Xingyun Lake, South-West China. J. Quat. Sci. 29 (7), 661–674.

Clark, P.U., Dyke, A.S., Shakun, J.D., Carlson, A.E., Clark, J., Wohlfarth, B., et al., 2009. The last glacial maximum. Science 325 (5941), 710–714.

Danielson, J.J., Gesch, D.B., 2011. Global multi-resolution terrain elevation data 2010 (GMTED2010) (No. 2011-1073). US Geological Survey.

Dortch, J.M., Owen, L.A., Caffee, M.W., 2013. Timing and climatic drivers for glaciation across semi-arid western Himalayan–Tibetan orogen. Quat. Sci. Rev. 78, 188–208.

Dutt, S., Gupta, A.K., Clemens, S.C., Cheng, H., Singh, R.K., Kathayat, G., Edwards, R.L., 2015. Abrupt changes in Indian summer monsoon strength during 33,800 to 5500 years BP. Geophys. Res. Lett. 42 (13), 5526–5532.

Fleitmann, D., Burns, S.J., Mangini, A., Mudelsee, M., Kramers, J., Villa, I., et al., 2007. Holocene ITCZ and Indian monsoon dynamics recorded in stalagmites from Oman and Yemen (Socotra). Quat. Sci. Rev. 26 (1–2), 170–188.

Fleitmann, D., Cheng, H., Badertscher, S., Edwards, R.L., Mudelsee, M., Göktürk, O.M., et al., 2009. Timing and climatic impact of Greenland interstadials recorded in stalagmites from northern Turkey. Geophys. Res. Lett. 36, L19707. https://doi.org/10.1029/2009GL040050.

Heyman, J., 2014. Paleoglaciation of the Tibetan Plateau and surrounding mountains based on exposure ages and ELA depression estimates. Quat. Sci. Rev. 91, 30–41. https://doi.org/10.1016/j.quascirev.2014.03.018.

Hou, J., D'Andrea, W.J., Wang, M., He, Y., Liang, J., 2017. Influence of the Indian monsoon and the subtropical jet on climate change on the Tibetan Plateau since the late Pleistocene. Quat. Sci. Rev. 163, 84–94.

Hu, G., Yi, C.L., Zhang, J.F., Liu, J.H., Jiang, T., Li, S.H., 2016. Late Quaternary glacial advances in the eastern Qilianshan, north-eastern Tibet, as inferred from luminescence dating of fluvioglacial sediments. J. Quat. Sci. 31 (6), 587–597.

Huffman, G.J., Bolvin, D.T., Nelkin, E.J., Wolff, D.B., Adler, R.F., Gu, G., et al., 2007. The TRMM multisatellite precipitation analysis (TMPA): quasi-global, multiyear, combined-sensor precipitation estimates at fine scales. J. Hydrometeorol. 8 (1), 38–55. https://doi.org/10.1175/JHM560.1.

Hughes, P.D., Gibbard, P.L., 2015. A stratigraphical basis for the Last Glacial Maximum (LGM). Quat. Int. 383, 174–185.

Jiang, G.Z., Gao, P., Rao, S., Zhang, L.Y., Tang, X.Y., Huang, F., et al., 2016. Compilation of heat flow data in the continental area of China (4th edition). Chin. J. Geophys.-Chin. Ed. 59, 2892–2910.

Jiang, Q., Ji, J., Shen, J., Matsumoto, R., Tong, G., Qian, P., et al., 2013. Holocene vegetational and climatic variation in westerly-dominated areas of Central Asia inferred from the Sayram Lake in northern Xinjiang, China. Sci. China Earth Sci. 56 (3), 339–353.

Johnsen, S.J., Clausen, H.B., Dansgaard, W., Gundestrup, N.S., Hammer, C.U., Andersen, U., et al., 1997. The $\delta^{18}$O record along the Greenland Ice Core Project deep ice core and the problem of possible Eemian climatic instability. J. Geophys. Res., Oceans 102 (C12), 26397–26410.

Kathayat, G., Cheng, H., Sinha, A., Spötl, C., Edwards, R.L., Zhang, H., et al., 2016. Indian monsoon variability on millennial-orbital timescales. Sci. Rep. 6, 24374.

Kirchner, N., Greve, R., Stroeven, A.P., Heyman, J., 2011. Paleoglaciological reconstructions for the Tibetan Plateau during the last glacial cycle: evaluating numerical ice sheet simulations driven by GCM-ensembles. Quat. Sci. Rev. 30 (1–2), 248–267. https://doi.org/10.1016/j.quascirev.2010.11.006.

Kong, P., Na, C., Fink, D., Huang, F., Ding, L., 2007. Cosmogenic $^{10}$Be inferred lake-level changes in Sumxi Co basin, Western Tibet. J. Asian Earth Sci. 29 (5–6), 698–703.

Kuhle, M., 1998. Reconstruction of the 2.4 million km2 late Pleistocene ice sheet on the Tibetan Plateau and its impact on the global climate. Quat. Int. 45, 71–108.

Lecavalier, B.S., Milne, G.A., Simpson, M.J., Wake, L., Huybrechts, P., Tarasov, L., et al., 2014. A model of Greenland ice sheet deglaciation constrained by observations of relative sea level and ice extent. Quat. Sci. Rev. 102, 54–84.

Li, S., Shi, Y., 1992. Glacial and lake fluctuations in the area of the west Kunlun mountains during the last 45 000 years. Ann. Glaciol. 16, 79–84.

Li, Y., Song, Y., Yin, Q., Han, L., Wang, Y., 2019. Orbital and millennial northern mid-latitude westerlies over the last glacial period. Clim. Dyn. https://doi.org/10.1007/s00382-019-04704-5.

Lifton, N., Beel, C., Hättestrand, C., Kassab, C., Rogozhina, I., Heermance, R., et al., 2014. Constraints on the late Quaternary glacial history of the Inylchek and Sary-Dzaz valleys from in situ cosmogenic $^{10}$Be and $^{26}$Al, eastern Kyrgyz Tian Shan. Quat. Sci. Rev. 101, 77–90.

Liu, Z., Lu, Z., Wen, X., Otto-Bliesner, B.L., Timmermann, A., Cobb, K.M., 2014. Evolution and forcing mechanisms of El Niño over the past 21,000 years. Nature 515 (7528), 550–553. https://doi.org/10.1038/nature13963.

Liu, Z., Otto-Bliesner, B.L., He, F., Brady, E.C., Tomas, R., Clark, P.U., et al., 2009. Transient simulation of last deglaciation with a new mechanism for Bølling-Allerød warming. Science 325 (5938), 310–314. https://doi.org/10.1126/science.1171041.

Maussion, F., Butenko, A., Champollion, N., Dusch, M., Eis, J., Fourteau, K., et al., 2019. The Open Global Glacier Model (OGGM) v1. 1. Geosci. Model Dev. 12 (3), 909–931.

Maussion, F., Scherer, D., Mölg, T., Collier, E., Curio, J., Finkelnburg, R., 2014. Precipitation seasonality and variability over the Tibetan Plateau as resolved by the high Asia reanalysis. J. Climate 27 (5), 1910–1927. https://doi.org/10.1175/JCLI-D-13-00282.1.

Mix, A.C., Bard, E., Schneider, R., 2001. Environmental processes of the ice age: land, oceans, glaciers (EPILOG). Quat. Sci. Rev. 20 (4), 627–657.

Murari, M.K., Owen, L.A., Dortch, J.M., Caffee, M.W., Dietsch, C., Fuchs, M., et al., 2014. Timing and climatic drivers for glaciation across monsoon-influenced regions of the Himalayan–Tibetan orogen. Quat. Sci. Rev. 88, 159–182.

Owen, L.A., Dortch, J.M., 2014. Nature and timing of quaternary glaciation in the Himalayan–Tibetan orogen. Quat. Sci. Rev. 88, 14–54. https://doi.org/10.1016/j.quascirev.2013.11.016.

Owen, L.A., Finkel, R.C., Haizhou, M., Barnard, P.L., 2006. Late Quaternary landscape evolution in the Kunlun Mountains and Qaidam Basin, Northern Tibet: a framework for examining the links between glaciation, lake level changes and alluvial fan formation. Quat. Int. 154, 73–86.

Peterse, F., Prins, M.A., Beets, C.J., Troelstra, S.R., Zheng, H., Gu, Z., et al., 2011. Decoupled warming and monsoon precipitation in East Asia over the last deglaciation. Earth Planet. Sci. Lett. 301 (1–2), 256–264.

Pritchard, H.D., 2019. Asia's shrinking glaciers protect large populations from drought stress. Nature 569 (7758), 649–654.

Rupper, S., Roe, G., Gillespie, A., 2009. Spatial patterns of Holocene glacier advance and retreat in Central Asia. Quat. Res. 72 (3), 337–346.

Saha, S., Owen, L.A., Orr, E.N., Caffee, M.W., 2018. Timing and nature of Holocene glacier advances at the northwestern end of the Himalayan-Tibetan orogen. Quat. Sci. Rev. 187, 177–202.

Saha, S., Owen, L.A., Orr, E.N., Caffee, M.W., 2019. High-frequency Holocene glacier fluctuations in the Himalayan-Tibetan orogen. Quat. Sci. Rev. 220, 372–400. https://doi.org/10.1016/j.quascirev.2019.07.021.

Shi, Y., 2002. Characteristics of late Quaternary monsoonal glaciation on the Tibetan Plateau and in East Asia. Quat. Int. 97, 79–91.

Webster, P.J., Yang, S., 1992. Monsoon and ENSO: selectively interactive systems. Q. J. R. Meteorol. Soc. 118, 877–926.

Weldeab, S., Rühlemann, C., Bookhagen, B., Pausata, F.S.R., Perez-Lua, F.M., 2019. Enhanced Himalayan glacial melting during YD and H1 recorded in the northern Bay of Bengal. Geochem. Geophys. Geosyst. 20, 2449–2461. https://doi.org/10.1029/2018GC008065.

Winkelmann, R., Martin, M.A., Haseloff, M., Albrecht, T., Bueler, E., Khroulev, C., Levermann, A., 2011. The Potsdam parallel ice sheet model (PISM-PIK)—Part 1: model description. Cryosphere 5 (3), 715–726. https://doi.org/10.5194/tc-5-715-2011.

Xu, X., Kleidon, A., Miller, L.E.E., Wang, S., Wang, L., Dong, G., 2010. Late Quaternary glaciation in the Tianshan and implications for palaeoclimatic change: a review. Boreas 39 (2), 215–232.

Yan, Q., Owen, L.A., Wang, H., Zhang, Z., 2018. Climate constraints on glaciation over high-mountain Asia during the last glacial maximum. Geophys. Res. Lett. 45 (17), 9024–9033.

Yan, Q., Zhang, Z., Wang, H., 2016. Investigating uncertainty in the simulation of the Antarctic ice sheet during the mid-Piacenzian. J. Geophys. Res., Atmos. 121 (4), 1559–1574.

Yao, T., Thompson, L., Yang, W., Yu, W., Gao, Y., Guo, X., et al., 2012. Different glacier status with atmospheric circulations in Tibetan Plateau and surroundings. Nat. Clim. Change 2 (9), 663–667. https://doi.org/10.1038/nclimate1580.

Zhang, E., Chang, J., Cao, Y., Sun, W., Shulmeister, J., Tang, H., et al., 2017. Holocene high-resolution quantitative summer temperature reconstruction based on subfossil chironomids from the southeast margin of the Qinghai-Tibetan Plateau. Quat. Sci. Rev. 165, 1–12.

Zhao, J., An, C.B., Huang, Y., Morrill, C., Chen, F.H., 2017. Contrasting early Holocene temperature variations between monsoonal East Asia and westerly dominated Central Asia. Quat. Sci. Rev. 178, 14–23.